IL NUOVO CIMENTO Vol. 31 C, N. 5-6 Settembre-Dicembre 2008
DOI 10.1393/ncc/i2009-10330-y

An experimental model of mixing processes generated by an array of top-heavy turbulent plumes

P. L. González-Nieto(1)(*), J. L. Cano(1) and J. M. Redondo(2)

(1) *Departamento de Física de la Tierra, Astronomía y Astrofísica II, Universidad Complutense de Madrid - Ciudad Universitaria s/n 28040, Madrid, Spain*
(2) *Departament de Fisica Aplicada, Universitat Politecnica de Catalunya Campus Nord UPC 08034, Barcelona, Spain*

(ricevuto il 30 Agosto 2008; approvato il 18 Marzo 2009; pubblicato online il 28 Aprile 2009)

Summary. — The mixing process of two fluids of unequal density generated by the evolution of an array of forced turbulent plumes is studied in the laboratory. The corresponding qualitative conclusions and the quantitative results based on measures of the density field and of the height of the fluid layers are described. The partial mixing process is characterized and analyzed, and the conclusions of this analysis are related to the mixing efficiency and the volume of the final mixed layer as functions of the Atwood number, which ranges from 0.010 to 0.134. An exponential fit is used to evaluate the mixing efficiency *versus* the Atwood showing the role of initial conditions on mixing efficiency variability.

PACS 47.27.-i – Turbulent flows.
PACS 87.57.N- – Image analysis.
PACS 92.60.hk – Convection, turbulence, and diffusion.

1. – Introduction

Turbulence is a complex motion which is characterized by highly effective mixing and transport processes. In many of the physical phenomena occurring in nature, for example, the diffusion of most physical quantities is governed by the mixing generated by turbulence. To properly understand atmospherical and oceanic turbulence, for example, a deep understanding of the mixing processes is first required.

This paper presents a study of turbulent mixing processes generated experimentally under an unstable density distribution in a fluid system. Our experimental set-up generates a discrete number of forced turbulent plumes whose behavior and interaction result in the mixing process. In this experiment our principal aim is the study of the properties

(*) E-mail: azufre2@hotmail.com

of the mixed fluid that is produced after the turbulent mixing process. Our interests lie in analysing the turbulent mixed regime because of the important implications that this regime has to geophysical studies.

Turbulent mixing as a result of unstable density stratification is especially relevant because local density overturning constitutes an essential part of the phenomena occurring in all stratified fluids [1]. If the fluids that constitute the unstable density stratification are miscible, as in our case, the turbulence will produce molecular mixing. This presupposes the action of energy dissipation mechanisms associated with small-scale turbulent eddies. Local unstable density stratifications occur when there is a density overturning in a stratified fluid. These unstable density stratifications correspond theoretically to a pure Rayleigh-Taylor instability [2-11]. This hydrodynamic instability appears in fluid systems placed in a gravitational field when the density of the system decreases in the direction of the gravity. The evolution of this kind of unstable system will usually generate a turbulent flow. The pure Rayleigh-Taylor instability can provide a fundamental theoretical model that may be used to approximate real-life situations. In fact, it is commonly used to simulate turbulent mixing. The hydrodynamic situation occurring in the experiment described in this paper is an unstable density distribution and, although it does not exactly correspond to a Rayleigh-Taylor situation, one may still use several of the theoretical concepts of the Rayleigh-Taylor instability as a reference.

The difficulties that hinder the direct investigation *in situ* of turbulent diffusion processes such as those occurring in the atmosphere, force us to use substitute methods such as laboratory techniques and experimental models to simulate natural phenomena. In experimental studies of real physical situations it is the hydrodynamic and convective similarities which serve as a basis for the relationship between real-life phenomena and the experimental model [12, 13].

In the following section, we provide a description of the experimental set-up; sect. **3** provides a detailed description of the qualitative features of the fluid flows generated experimentally, as well as the observed mixing process; sect. **4** presents the quantitative results related to the global characteristics of the mixing process, such as the height of the mixed layer h_M and the mixing efficiency η whose definition will be explained in sect. **4** and it is

$$\eta = 1 - \frac{(\Delta Ep)_{\text{partial}}}{(\Delta Ep)_{\text{nomix}}}\,. \tag{1}$$

Finally, the conclusions of our investigation are presented.

2. – Experimental method

There exist different procedures to obtain experimentally unstable density interfaces. Some examples of these procedures are: the use of unmixable fluids, employment of small width containers, or production of stable interfaces which are subjected to an acceleration directed from the less dense fluid to the denser one [2-5]. Here we describe a new experimental method to obtain an unstable density distribution.

The experimental apparatus used was designed by the authors and was built in the research support workshops of the Complutense University of Madrid (UCM). The experimental fluids are sodium chloride solutions which were considered as incompressible. These solutions are thoroughly miscible and as such, present a high Schmidt number, of the order of 10^3.

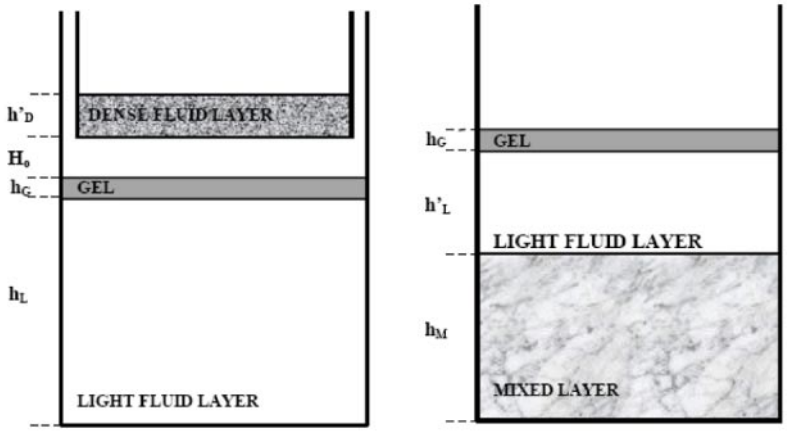

Fig. 1. – Schematic diagram of the experimental set-up which shows the initial and final states of the fluid system. The light layer height h_L is 12.7 cm and ρ_L is the density of the lighter fluid; the gel layer height h_G is 2 cm and ρ_G is its density; the boxes system height H_0 is 1.5 cm; the dense layer height h'_D is 1.06 cm and ρ_D is the density of the dense fluid layer; h_M is the mixed layer height and h'_L is the final light layer height. Representation not in scale.

The fluid system consists of three homogeneous fluids with different densities that are initially at rest. The fluids are inside a cubic glass container of sides 270 mm (fig. 1). At the bottom of the container there is a fluid with lower density ρ_L making a layer designated as the "light layer" with a height h_L. On top of this layer, a sodiumcarboximethyl cellulose gel stratum, or CMC gel [14, 15], is placed with density ρ_G and a height of h_G. Finally, a system made of two metacrylic boxes, one fitting inside the other, is placed at a height H_0 from the CMC gel layer. The bottoms of the boxes are pierced with orifices that have apertures that can be regulated. These boxes contain the fluid of greater density ρ_D which constitutes the "dense layer". The dense fluid reaches a height h'_D inside the boxes and is colored with sodium fluorescein which acts as a passive tracer. It should be mentioned that the density of the lighter fluid was pre-determined in relation to the density of the CMC gel so that a stable density interface is created between these two fluids (fig. 1).

The height H_0 which separates the system of boxes from the CMC gel layer is occupied by air. This height H_0 increases the overall initial potential energy of the fluid system. The role of this increase in energy will be analyzed in sect. **4**. The experiments were always performed with the same number of orifices in the boxes and with a fixed height H_0 whose value is 1.5 cm.

One purpose of the presence of the CMC gel in the laboratory model is to represent in a faithful way real situations in which the unstable layers are separated by stable zones such as in the atmosphere. Another reason is the practical advantage of slightly delaying the mixing process so that it may better be observed experimentally. The presence of the gel stratum influences the energy balance of the fluid system as well, and will also be analyzed quantitatively in sect. **4**.

Placing of the CMC gel layer on top of the light layer is accomplished through a metallic mesh basket with dimensions adjusted to those of the experimental container. The basket is handled through a motor and a pulley system and involves an important difficulty because of the special characteristics of the gel, a non-Newtonian fluid with a

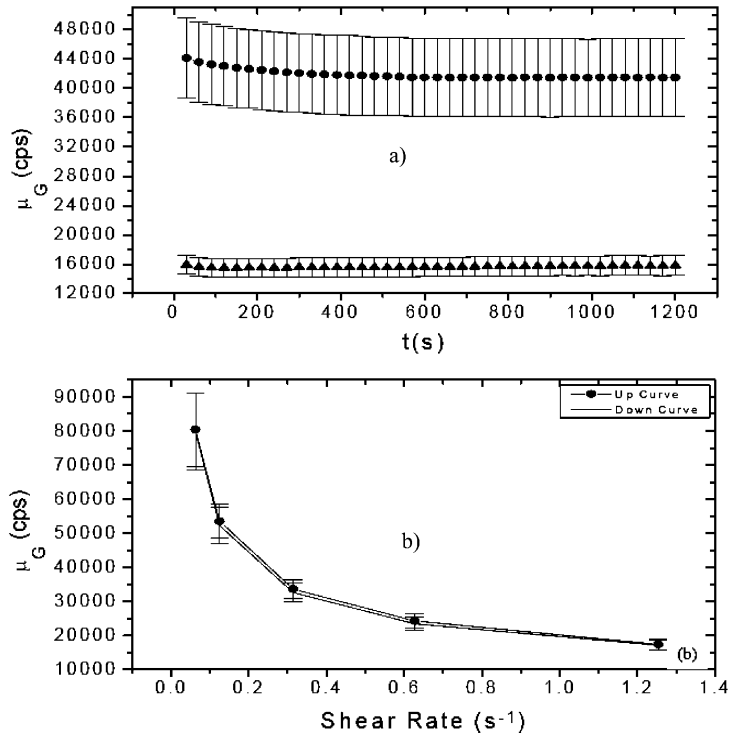

Fig. 2. – Thyxotropic behaviour of the sodiumcarboximethyl gel. (a) Time evolution of the gel viscosity for the more viscous gel (•) and for the less viscous one (▲) with a rotation speed of 0.6 rpm. (b) Evolution of the gel viscosity with the shear rate for the less viscous gel.

large viscosity [14]. It is essential to avoid the breakup of the gel layer and its thickness must be as uniform as possible so that the dense layer always goes through the same distance of gel.

The sodiumcarboximethyl celulose gel is obtained through the dissolution of the carboximethyl salt in water. A stirring-rod (Miralles trademark) is used at rotation speeds between 1000 and 1500 rpm. Two CMC gels with different viscosity but with similar thyxotropic behavior were used [14]. This behavior is shown in fig. 2. The most viscous gel, or gel 1, has an average viscosity of 4.3×10^4 cP and a density of $1.030\,\mathrm{g/cm^3}$. The less viscous gel, or gel 2, has a density of $1.025\,\mathrm{g/cm^3}$ and an average viscosity of 1.7×10^4 cP.

The CMC gel is a non-Newtonian time-dependent fluid and, as mentioned, presents a thyxotropic behavior, *i.e.* its viscosity decreases with time as long as it is submitted to a constant shear. Experimental data from the dynamic viscosity of the gels was measured using a rotational viscosimeter (Brookfield Model DV-II) and is shown in fig. 2. Figure 2a shows the time evolution of viscosity when the shear rate applied to the CMC gel is kept constant because the rotation speed of the rotational element of the viscosimeter has a value of 0.6 rpm. Figure 2b shows the gel behavior when it is submitted to a sequence of increasing and later decreasing rotation speeds until the speed is returned to the starting point. It is interesting to note that the up and down curves do not coincide and, indeed,

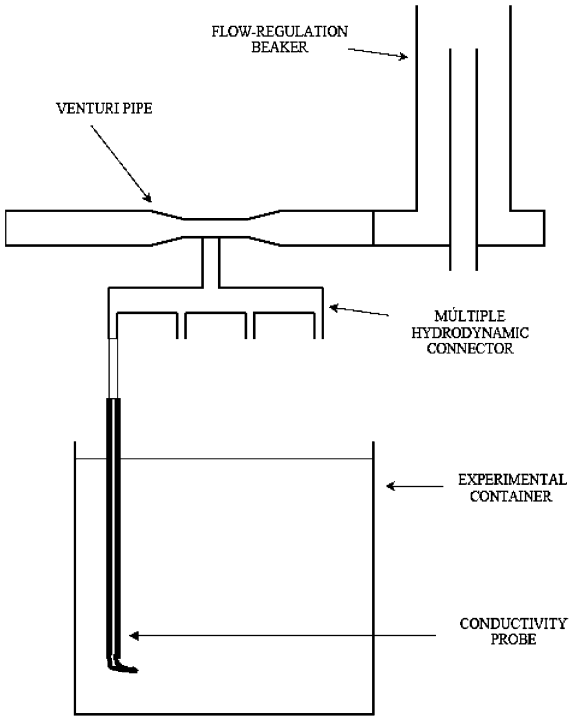

Fig. 3. – Schematic diagram of the suction system for the conductivity probes. It is composed of a flow-regulation beaker, a Venturi meter and a multiple hydrodynamic connector.

trace a small hysterisis cycle due to the decrease of viscosity with time. From these figures, we can deduce that the CMC gels used are slightly thyxotropic.

The experiment begins when the orifices of the box system are switched to the open position, then the dense fluid flows from the system of boxes and it is injected through the orifices pierced in the bottoms of the boxes because there is a pressure change. The dense fluid flows as jets through the air layer and these dense fluid jets come into the gel layer. Therefore the denser fluid impinges on the CMC gel layer and goes through the gel locally arriving in the shape of jets which break down the surface tension of the gel. The high viscosity of the gel and the small width of the gel layer make the dense fluid flow in the laminar regime. As a consequence, the dense fluid flows through the gel as jets again and it comes into the lighter fluid layer. The result is the generation of several forced plumes which are gravitationally unstable. The development of these plumes makes the turbulent mixing process possible and will be described in the following section. The orifice diameter affects the initial properties of the turbulent plumes increasing their moment and bulk flow [16]. There is no mixing between the denser fluid and the CMC gel.

The evolution of the density field is measured by a multichannel conductivimeter which has previously been calibrated. This instrument was built in the research support workshops of the UCM according to the original design by John Mumford of the Engineering Department of Cambridge University [17]. The conductivimeter record is controlled by an analogous-digital converter Unidata Starlogger Model 6004B and the output data are stored in a computer.

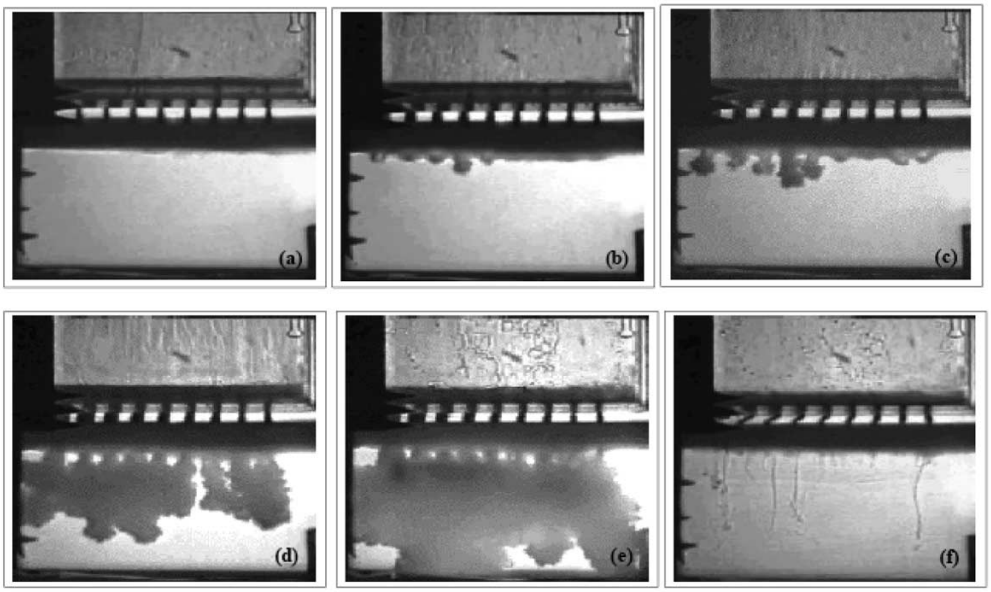

Fig. 4. – Time evolution of a partial mixing process through its frames sequence. Experiment made with the less viscous CMC gel and Atwood number equal to 0.130. (a) Initial experimental state (0 s). (b) Starting of turbulent plumes (0.24 s). (c) Development of the turbulent plumes (0.32 s). (d) Lateral and front interactions between the turbulent plumes (0.64 s). (e) Interaction of the fluid system with the physical contours of the container (1.00 s). (f) Final state after the partial mixing process (96.70 s).

Four suction conductivity probes, which are located at different heights within the fluid system, are connected to the conductivimeter [17, 18]. The correct functioning of the conductivity probes requires the use of a suction system composed of a flow-regulation beaker, a Venturi pipe and a multiple hydrodynamic connector (fig. 3). The flow-regulation beaker is a device which controls the input mass flow in the Venturi meter, and the Venturi pipe acts as a small suction pump. The hydrodynamic connector permits the simultaneous connection of the four conductivity probes to the same Venturi pipe so that their suction mass flow will be approximately equal.

The evolution of the fluid flow is visualized by the shadowgraph technique or directly by fluorescence induced by light. All the experiments are recorded by a video camera for their subsequent digitalization carried out by two image softwares: DigImage and Adobe Première 5.1. The software permits frame recording such as the ones shown in figs. 4, 5 and 6 where these images correspond to the time evolution of different turbulent mixing processes.

The present work is based on 150 experiments done at room temperature. The number of repetitions of each experiment oscillates between a minimum of 5 and a maximum of 10. The experimental conditions were modified through the use of two CMC gels with different viscosities and a total of 20 different saline solutions to constitute the denser fluid layer. As the density of the denser fluid changed, the Atwood number and the initial buoyancy of the fluid system changed with it. The density ratio between the lighter fluid and the denser one provided a wide range of Atwood numbers which extended from 0.010 to 0.134, where ρ_D/ρ_L is nearly unity. The Atwood number A is defined as a function

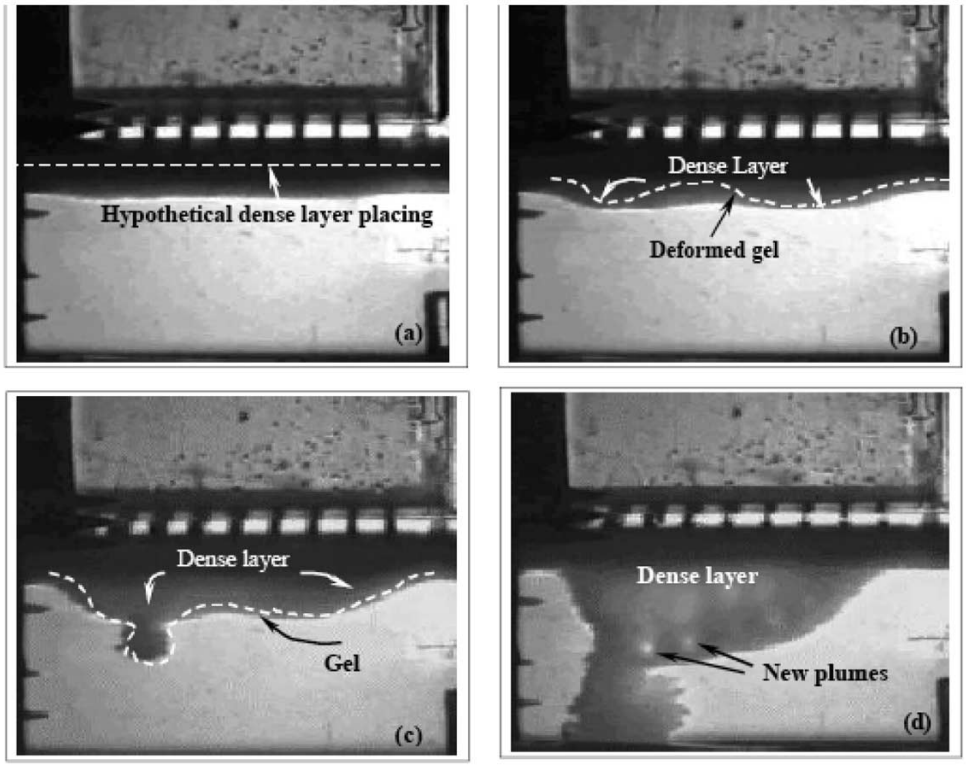

Fig. 5. – Time evolution of a partial mixing process corresponding to an experiment made with the more viscous CMC gel and Atwood number equal to 0.130. (a) Small protuberance in the CMC gel layer (0.32 s). (b) Appearance of two gel protuberances which fill up with the denser fluid (0.60 s). (c) Break-up of one of the protuberances through a turbulent plume (1.01 s). (d) Simultaneous growth of the plume and the protuberance which is emptying and distorting the CMC gel layer at the same time. New turbulent plumes begin (1.61 s).

of the magnitudes described before as follows:

$$A = \frac{\rho_D - \rho_L}{\rho_D + \rho_L} \,. \tag{2}$$

The following is a qualitative description of the turbulent mixing process; sect. **4** will describe the global quantitative results.

3. – Qualitative results

After the denser fluid has gone through the gel layer there appears an array of forced plumes which are gravitationally unstable. As the turbulent plumes develop, the denser fluid comes into contact with the lighter fluid layer and the mixing process between them begins. The behavior of this fluid system is governed by the turbulent energy source generated by the buoyancy under the Boussinesq approximation [13]. The influence of the initial conditions is shown by the different types and number of turbulent plumes

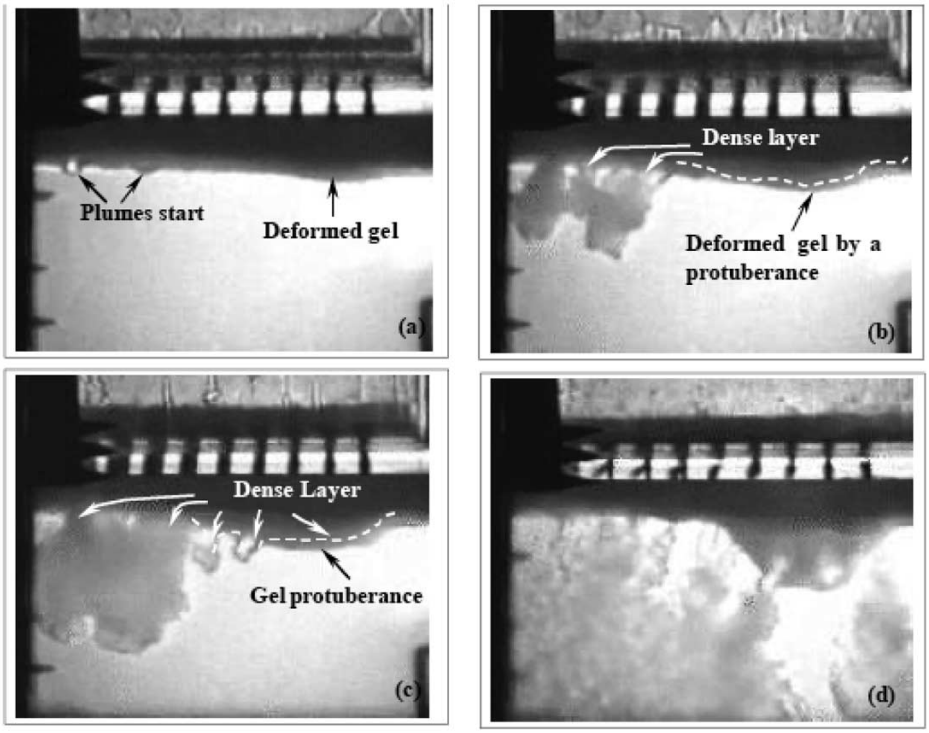

Fig. 6. – Time evolution of a partial mixing process corresponding to an experiment made with the less viscous CMC gel and Atwood number equal to 0.037. (a) Slight protuberance in the CMC gel layer and an incipient formation of some turbulent plumes (0.32 s). (b) Simultaneous development of the plumes and the CMC gel protuberance (0.64 s). (c) Growth of the plumes and break-up of the protuberance through two plumes (1.00 s). (d) General interaction between plumes while the protuberance break-up continues through other plumes (3.32 s).

(figs. 4, 5 and 6) and the development of these depends on the experimental conditions. Specifically, it depends on three factors which will be discussed separately: first, the CMC gel used which has viscosity ν_G; second, the ratio of densities of the fluid system, or Atwood number A.

The third factor that influences the overall mixing produced by the convective situation of the array of plumes penetrating the gel or without it, is the direct geometrical effect that the initial conditions (separation and size of the plume holes) have over the volume where mixing can take place. The array of holes is composed by six files and eight columns. The effect of the gel on the final distribution of plume number and sizes is to randomise the distribution of the well-established pattern used in most of the experiments.

Of course this initial configuration as a regular array of plumes would only apply exactly in the case of experiments without gel. Other experiments with a different number and distribution of holes have been made and their results will be published in the future. Because mixing has only occurred in a small fraction of the volume, *i.e.* the cone volume of height h divided by the product of the tank base area, S, times h, the maximum mixing efficiency defined below will be about 0.25. On the other hand, the case of experiments

such as those of the plate removal type of Linden and Redondo (1991) would be equivalent to many small and very close holes that occupy almost the same area as the base of the tank, then the maximum mixing efficiency is 0.5.

In the case of another particular distribution of plumes the ratio of the volume where mixing is impossible (*i.e.* the volume between the plume array) to the whole possible mixing volume is a limiting factor on the maximum mixing efficiency.

As the gel viscosity is reduced, the probability of initial generation of some gel protuberances reduces, so that the probability of the formation of turbulent plumes increases. This behavior is clearly shown in figs. 4, 5 and 6 which show frame sequences corresponding to the time evolution of several turbulent mixing processes visualized with the shadowgraph technique. Figure 4 shows the time evolution of a turbulent mixing process where the CMC gel used is the less viscous one and the Atwood number is the same as in fig. 5 ($A = 0.130$). Figures 4c, 4d and 4e correspond to the same time sequence as, respectively, figs. 5a, 5b and 5c. If we compare these figures we observe clearly the initial absence of turbulent plumes and the appearance of the mentioned gel protuberances in figs. 5a and 5b because the gel viscosity has increased. These protuberances grow as they fill up with the denser fluid (figs. 5b and 5c) until they burst, releasing the denser fluid and generating plumes with slopes that are not necessarily vertical (fig. 5c). Figure 6 shows that these two phenomena, protuberances and plumes, are not mutually excluding. Here, the corresponding Atwood number is 0.037 and the CMC gel used is the one with the least viscosity.

The other factor having an effect on the fluid flow which shall be discussed next is the Atwood number A. This adimensional parameter represents the strength of the buoyancy effect as a consequence of the density difference between the fluids. The greater the value of the Atwood number, the more the available potential energy for the mixing process. This implies a greater quantity of mixed fluid, and therefore, a greater height of the mixed layer. In addition, this results in a greater mixing efficiency as will be verified in the following section.

Figure 6 shows the time evolution of a mixing process whose Atwood number is 0.037, approximately one third of the value corresponding to the experiment represented in fig. 4. The CMC gel is the same in figs. 4 and 6. Figures 4c, 4d and 4e correspond to the same time lapse as, respectively, figs. 6a, 6b and 6c. Comparing these figures we observe that the rates of the turbulent plumes are greater in fig. 4 than in fig. 6. This is simply because the Atwood number is greater as explained before.

The mixing process may be considered to be formed by three stages: initial, intermediate and final stage. The initial phase of the process (figs. 4a, 4b, 5a, 5b, 5c, 6a and 6b) depends on the Atwood number and on the CMC gel viscosity as mentioned before. This initial stage of the partial mixing process is governed by the axysimetric and forced turbulent plumes [16, 19] which cause the process to be three dimensional. The downward speed of the plume produces an upward recirculation movement in the lighter fluid which favours the mixing. Furthermore, there is entrainment of the ambient fluid that is directed through the profile of the turbulent plumes [19].

The sides of the plumes are zones with strong shears which generate Kelvin-Helmholtz instabilities. Secondary Rayleigh-Taylor instabilities may also appear in the front of the convective plumes. All these instabilities generate small disturbances which erode the sides and the front of the turbulent plumes. The greater part of the molecular mixing is a consequence of these small-scale instabilities which superimpose on the greater scale structures. This is a characteristic phenomenon of mixing processes in stratified fluids [20]. In fact, the results obtained by other researchers, based on the analysis of

their experimental digitalizations, indicate that the density variations are smaller inside a fluid structure than on its contours [7].

The second, or intermediate stage, is characterized by the vertical development of the turbulent plumes (fig. 4c) and by the lateral interaction between them (figs. 4d and 6c). As a consequence of this interaction, a single convective front appears in which the fluid structures lose their individuality. The development of these plumes is limited by the physical contours of the experimental container so that as they reach the bottom (figs. 4e and 6d) the fluid system overturns. Under these conditions, the mean stratification of the fluid system is more uniform with respect to the initial state.

The final stage is characterized by the fine microstructure turbulence and by the appearance of a stable density interface which sets the upper limit on the mixed layer (fig. 4f). In this stage there is a decrease in the density difference of the fluid system, as compared to the initial density difference, because the small-scale turbulence contributes decisively to the mixing. Moreover, the final mixed layer which has a stable density stratification appears clearly in this final stage. Since there is a stable stratification, a fraction of the available energy is employed to work against the buoyancy forces and internal waves that may be generated which damp with time [21]. Under this situation the density fluctuations attenuate and the turbulent microstructure decays until it disappears.

The final result of the mixing process is a mixed layer located at the bottom of the experimental container (fig. 4f) which is separated from the unmixed lighter fluid by means of the stable density interface already mentioned. Since not all of the lighter fluid participates in the mixing, we qualify it as a partial mixing process. On the other hand, the mixed layer obtained experimentally is not homogeneous, but has a density stratification.

Summing up, we have axysimetric turbulent plumes at the initial stage which develop at the intermediate stage. This development is caused by the lateral interaction between the plumes. At the final stage the turbulent mixing decays, leading to the appearance of a mixed layer that has a stable density stratification.

4. – Global quantitative results

In this section we analyze two global properties of the partial mixing process: the mixing efficiency and the mixed layer height. These properties are those that exclusively depend on the characteristics of the fluid system in the initial and final states. As the final mixing process is influenced by the initial buoyancy, the mixing efficiency η and the mixed layer height h_M (see fig. 1) are analyzed *versus* the Atwood number A which is proportional to the buoyancy-driven forcing. In addition, these two global properties η and h_M are influenced experimentally by the height of the denser fluid H_0 and the presence of the CMC gel. Therefore, the influence of these last two experimental parameters is also discussed.

The height H_0 is due to the experimental set-up because we place the denser fluid on the CMC gel layer by means of two boxes with regularly distributed holes. This system of boxes and the CMC gel are separated by a layer of air. Therefore, H_0 is the width of this air layer, it is also the height of the boxes relative to the gel layer and, finally, it is the initial height of the denser fluid relative to the gel layer. Moreover, the presence of the height H_0 is directly related with the role of initial conditions on the mixing efficiency. In general the change in initial conditions of a mixing process is not irrelevant because this is one of the fundamental problems of the understanding of mixing. Actually we do

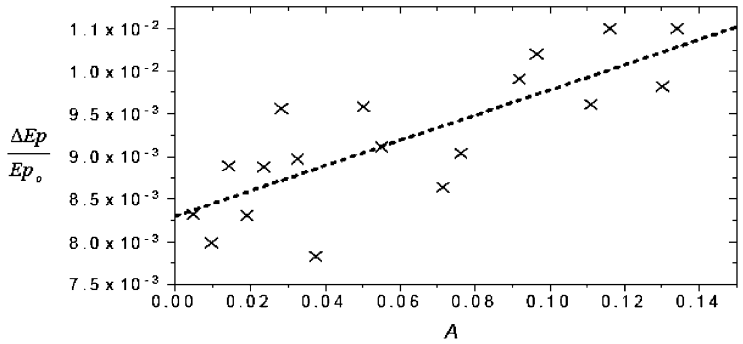

Fig. 7. – Relative increment of the initial potential energy $\Delta E_p/E_{p0}$ *vs.* the Atwood number, A. The dashed line is only drawn for comparison and it is given by the following expression: $(\Delta E_p/E_{p0}) = 0.015\,A + 0.008$ and with a regression coefficient $r = 0.80$.

not consider the effect of the change of this initial condition H_0 on the mixing because the experiments were always performed with the same height H_0. But, we are in perfect condition to do it at future because the height H_0 can be easily changed experimentally.

Experiments were made without the system of boxes and it was deduced that the physical and dynamical development of the process is not influenced in an essential way by the use of this box system. The development of the fluid flow is only influenced by the initial physical characteristics of the fluid layers (the Atwood number, the gel viscosity and the heights of the layers). Finally, all the experiments were always performed with the same fixed height H_0 which has a value of 1.5 cm.

The height of the system of boxes H_0 increases the initial potential energy of the dense fluid layer if we compare it with that the dense fluid would have if it is on the CMC gel. Therefore, the effect of the height H_0 is manifested by an increase in the available initial potential energy of the fluid system. We can compare the available initial potential energy of the fluid system with and without the height H_0 and the result of comparing is named ΔE_p. If we refer this change ΔE_p to the initial potential energy of the fluid system with the height H_0, named E_{p0}, we get the relative increment of the initial potential energy $\Delta E_p/E_{p0}$. As H_0 is constant, we could think that the increase of the initial potential energy of the fluid system is constant. But this increase of the potential energy changes potentially to the Atwood number changed mainly by density difference of the brine—the denser fluid—as fig. 7 shows. The amount of increase in the initial potential energy ΔE_p depends on the Atwood number and is on the order of 1.5%. Figure 7 shows the relative increment of the initial potential energy $\Delta E_p/E_{p0}$ *versus* the Atwood number A. As this adimensional number goes to zero or for low Atwood numbers there is not enough stuff for the potential energy associated with H_0 to mix. The dashed line is a linear fit which mathematical expression is: $(\Delta E_p/E_{p0}) = 0.015\,A + 0.0083$ with a regression coefficient $r = 0.80$. This dashed line is only drawn for comparison and it gives a qualitative idea of growth of the relative increment of the initial potential energy with the Atwood number. About the dispersion in the points, we want to say that this dispersion is not statistically important because the statistical validity is greater than 99% for the number of data and the number of freedom degrees we used.

As mentioned, the final state of the fluid system is characterized by the presence of a stable density stratification which appears because the mixed layer is separated from

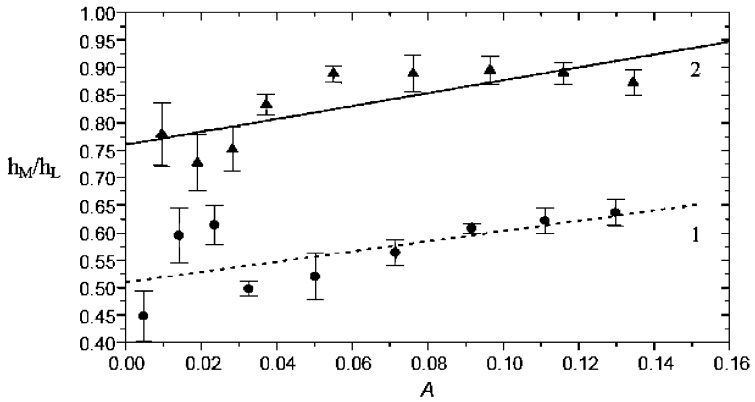

Fig. 8. – Behavior of the adimensional height of the mixed layer with the Atwood number for experiments made with the more viscous CMC gel (Curve 1, •), and with the less viscous one (Curve 2, ▲). The figure shows the linear fits done.

the unmixed lighter fluid by a stable density interface. The mixed layer height h_M represents the final height of this stable density interface (see fig. 1) and was measured experimentally. Of course, the height h_M is directly proportional to the final quantity, or volume, of the mixed fluid. In order to analyze this height h_M quantitatively we first make it adimensional and divide it by the sum of the height h_L of the light fluid layer and the height h'_D of the denser one. The purpose of this is to facilitate the comparison among experimental results obtained under different initial and boundary conditions. Moreover, the range of the mixed layer height h_M is automatically normalized to one and becomes independent of the system of units used. Qualitatively, the mixed layer height would increase as the Atwood number grows because h_M represents the volume of the mixed fluid; in other words, as the buoyancy effect increases so does the convective turbulent mixing.

Figure 8 shows the adimensional mixed layer height h_M *versus* the Atwood number and the empirical fits to the data for this height. A linear fit was chosen because it adequately represents the global growth trend of this height with the Atwood number. The expressions for the corresponding fits are

$$\begin{aligned} \left(\frac{h_M}{h_L+h'_D}\right)_1 &= 0.90A + 0.50, \\ \left(\frac{h_M}{h_L+h'_D}\right)_2 &= 1.10A + 0.70. \end{aligned} \tag{3}$$

Here, as before, the subindex 1 makes reference to the more viscous gel and 2 to the less viscous one. The first fit has a confidence level of 90%, whereas the second one has a 95% confidence level. These confidence levels have been deduced from the regression coefficients $r_1 = 0.64$ and $r_2 = 0.80$.

In fig. 8 the effect of the CMC gel viscosity may also be observed: the mixed layer height h_M increases if the gel used is the less viscous one. One reason for this increase in height is the greater number of turbulent plumes that appears when the gel viscosity is reduced. Another reason for this behavior is the increase of the downward velocity of turbulent plumes which generates greater shears in their edges favouring the mixing and thereby increasing the mixed layer height.

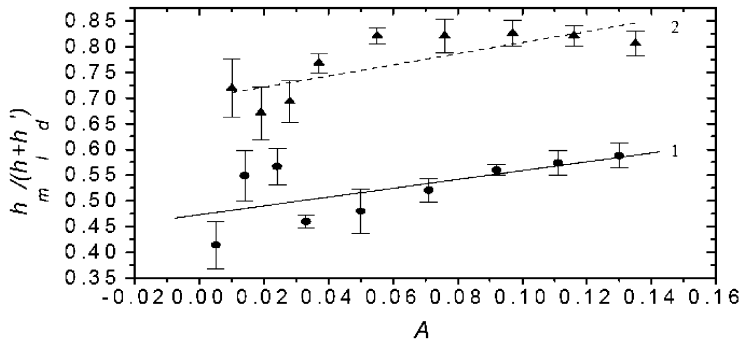

Fig. 9. – Behavior of the adimensional height of the mixed layer with the Atwood number. Curve 1 corresponds to experiments done with the more viscous gel and curve 2 corresponds to experiments made with the less viscous gel.

From the results of fig. 8 we may deduce that the gel removes a certain amount of energy from the downward-flowing denser fluid. This energy is employed in overcoming the viscous tension of the gel. To determine experimentally what effect the presence of the gel has, experiments were done under the exact same experimental conditions (fig. 1) except for the absence of the CMC gel layer. The height of the final mixed layer was measured experimentally and, as might be expected, it was greater than in the case that included the gel; this is shown in figs. 9 and 10. The mixed layer height changes 18% for the least viscous gel and 44% for the most viscous one with respect to the experiments without gel, agreeing with the idea that the gel absorbs some of the energy. There is a reduction in the kinetic energy of the down-flowing denser fluid which results in a delay in the mixing process of about 1% in time. Since the duration of the whole experiment is of the order of four minutes, this would amount to a delay of approximately a second.

As mentioned before, the denser fluid and the lighter one do not mix completely which implies that the mixing process is only partial. Here, the mixing efficiency η of this process is analyzed, where η is defined as the fraction of the available energy that is used to mix the fluids. The values of the mixing efficiency are obtained from the potential energy change that occurs during the mixing process. This potential energy variation is computed through the comparison of the initial and final density profiles of the fluid system which are measured from experimental parameters of the initial and final states of the fluid system only. Therefore, as the mixing efficiency is a global quantity we do not need to use the intermediate density profiles measured experimentally. The time evolution of vertical mean density profiles for experiments made with both CMC gels for Atwood numbers $A = 0.010$ and $A = 0.134$ were compared. The vertical density profiles approximated by linear fits to the experimental data and although the final density profiles are not exactly linear, their evolution is useful to characterize the time evolution of density profiles globally by means of a single slope change in time. We think that these fits also help to understand what happens [18].

The definition of the mixing efficiency η is [6, 7]

$$\eta = 1 - \frac{(\Delta Ep)_{\text{partial}}}{(\Delta Ep)_{\text{nomix}}}, \tag{4}$$

where $(\Delta Ep)_{\text{partial}}$ is the actual variation of potential energy associated to the partial mixing process. $(\Delta Ep)_{\text{nomix}}$ is the potential energy change of a process without mixing in

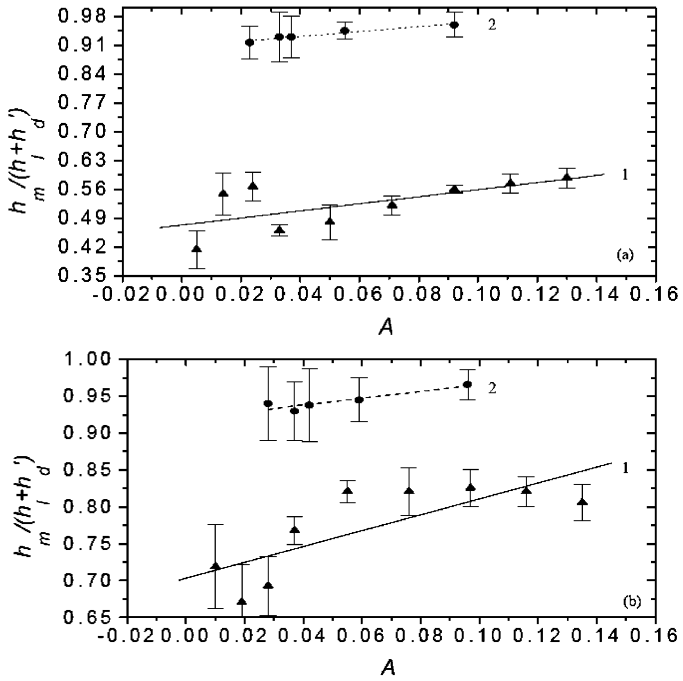

Fig. 10. – Behavior of the adimensional height of the mixed layer with the Atwood number. (a) Curve 1 corresponds to experiments done with the more viscous gel and curve 2 to experiments without gel. (b) Curve 1 corresponds to experiments made with the less viscous gel and curve 2 to experiments done without gel.

which the denser fluid and the lighter one only exchange positions. The mixing efficiency presented is like an *extrapolation* from the Rayleigh-Taylor situation because our fluid system is unstable stratified and the mixing process is only made between the denser fluid layer and the lighter one as in a Rayleigh-Taylor experiment. The gel does not suffer any mixing process. Therefore the mixing efficiency is evaluated from the energy change that occurs during the mixing process and which is due to the denser-lighter fluid mixing. This is true for our experimental set-up and for the Rayleigh-Taylor experiment.

We study the mixing efficiency under two kinds of mixed layer: homogeneous and stratified with two layers as fig. 11 shows. Figure 11(a) represents the final configuration of the fluid system if we consider a homogeneous mixed layer. This situation is not real because we do not get this final state experimentally. But we consider this configuration because is important to the analysis we make. Figure 11(a) is used to derive the expression in eq. (5). Figure 11(b) represents the final state of the fluid system if we consider a stratified mixed layer. This situation is the real one because we get it experimentally, we get a mixed layer which it is stratified. Figure 11(b) is used to derive expression (6).

If the mixed layer is considered homogeneous, the mixing efficiency has the following expression:

$$\eta_H = \frac{\Delta h_L}{2h_L} \frac{1}{1 + \left(\frac{\rho_G - \rho_D}{\rho_L - \rho_D}\right) \frac{h_G}{h_L} + \left(\frac{\rho_D}{\rho_L - \rho_D}\right) \left(\frac{h_D - h'_D}{2h_L} - \frac{H_0}{h_L}\right)} . \tag{5}$$

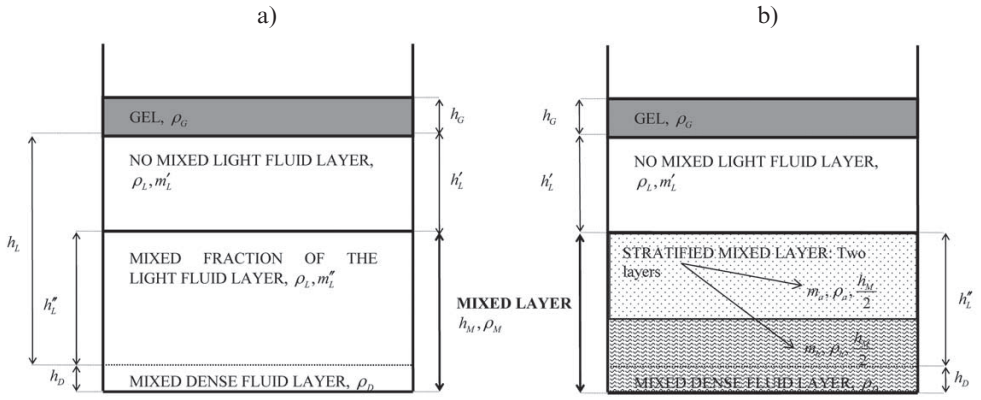

Fig. 11. – Schematic diagram of the final states of the fluid system. (a) It represents the final configuration if we consider a homogeneous mixed layer which is not real but theoretical important. (b) It represents the final state if we consider a stratified mixed layer which is the real situation we get experimentally. Notation: the gel layer height is h_G and ρ_G is its density; the boxes system height is H_0; ρ_L is the density of the lighter fluid and h'_L is the final light layer height; h_M is the mixed layer height. Representation not in scale.

This expression is derived from eq. (4) taking into consideration the characteristics of the experiment (see fig. 1 and 11(a)). The magnitude $\Delta h_L = h_L - h'_L$ is the difference between the initial and final thickness of the light layer (fig. 1) and h_D is the height the denser fluid would have if it was located inside the experimental container.

In our experiment, the mixed layer is stratified because mixing is not complete ($\eta = 0.5$). From observations of the final density profiles that showed a strong density step, we assume that the stratification is made up by two layers. We make this approximation because we know experimentally that the final density profile was not constant—and we cannot determine experimentally if it is linear—but exhibited a strong density gradient with a layer of almost light fluid on top of a heavier and well-mixed layer. This has been found to be due to the interpenetration of the unstable plumes only through a fraction of the area at the top, precisely because once the dense fluid looses its potential energy it may not mix with the lighter fluid above.

If the mixed layer is considered stratified, then the corresponding mixing efficiency has the following expression:

$$\eta_E = \frac{\eta_H}{2} - \frac{\frac{\Delta h_L \rho_L}{4h_L(\rho_L-\rho_D)}\left(\frac{\Delta h_L}{h_D} - \left(\frac{\Delta h_L - h_D}{\Delta h_L}\right)\left(1+\frac{\Delta h_L}{h_D}\right)\right) - \frac{\rho_D h_D}{4h_L(\rho_L-\rho_D)}}{1+\left(\frac{\rho_G-\rho_D}{\rho_L-\rho_D}\right)\frac{h_G}{h_L} + \left(\frac{\rho_D}{\rho_L-\rho_D}\right)\left(\frac{h_D-h'_D}{2h_L} - \frac{H_0}{h_L}\right)}. \tag{6}$$

This expression is also deduced from eq. (4) taking into consideration the characteristics of the experiment (see fig. 1 and 11(b)).

Figures 12a and 12b show a graphical comparison between the average mixing efficiency when the final mixed layer is considered as homogeneous, and the average mixing efficiency corresponding to a two-layer profile. We observe that, independently of the gel viscosity, the efficiency associated to the stratified mixed layer is always less than the efficiency corresponding to the homogeneous case. The lack of mixing is reflected in a stably stratified layered system at the end of the overturning process, this may be

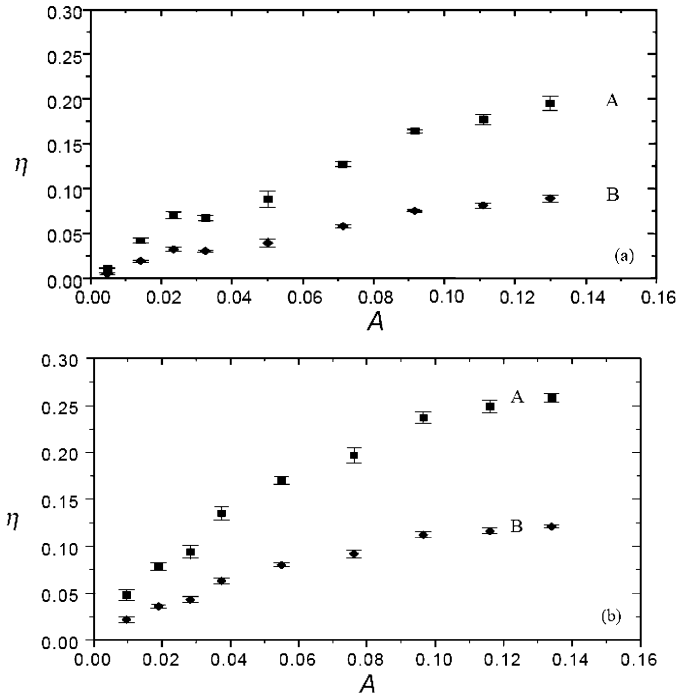

Fig. 12. – Behavior of the mean mixing efficiency *vs.* the Atwood number considering the mixed layer homogeneous (Curve A, ■) and stratified with two layers (Curve B, ⧫). (a) Experiments made with the more viscous CMC gel. (b) Experiments made with the less viscous CMC gel.

produced by either the initial condition effect of the discrete plume array that is only able to mix in a fraction of the tank volume or by the direct effect of the Atwood number that controls the available potential energy at the beginning of the experiment. In the events with very small mixing efficiency the overturning process also produces internal waves that reduce even more the energy available for mixing as described by Redondo [22].

Other scientific works state that the maximum mixing efficiency is reached when the final profile is totally mixed and homogeneous. This value is 0.5; if the final profile is stratified, as it is in our case, then the mixing efficiency is calculated about 0.17 [23]. We agree with other researchers that one must concentrate more on the overall mixing efficiency behavior in relation to the Atwood number than on the exact numeric values [21, 24] but here we may measure the effects of different initial conditions [25]. Moreover, one must have in mind that the laboratory model does not correspond exactly to a Rayleigh-Taylor instability and, therefore, its efficiency values are only taken as a reference.

As mentioned before, experiments without the gel were made; the percentage variation of the mixing efficiency η was analyzed under these new conditions. It was deduced that the maximum change of the efficiency, in percentage, between the case *with* and the case *without* the gel amounts to 60% for the most viscous gel.

In fig. 13 we plot the average mixing efficiency as a function of the Atwood number of the fluid system. This mixing efficiency corresponds to the case of the stratified mixed layer. In general, we observe that the efficiency increases as the Atwood number A grows.

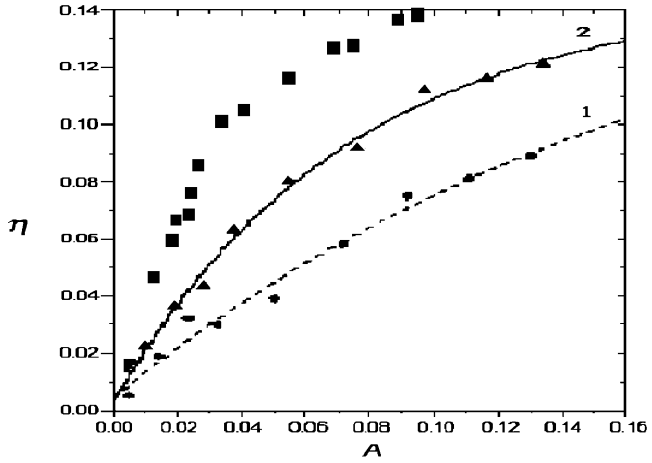

Fig. 13. – Mean mixing efficiency *vs.* the Atwood number for experiments made with the more viscous CMC gel (Curve 1, •), and with the less viscous one (Curve 2, ▲). The mixed layer is stratified. The corresponding empirical fits are shown.

Physically, the increase in Atwood number implies that the buoyancy effect grows, as does the convective acceleration. Therefore it produces a greater mixing process with a higher efficiency associated with it. There is a smooth increase in the mixing efficiency with the Atwood number which is also present in other scientific work [7].

Curve 2 of fig. 13 shows experiments done with the less viscous gel. These experiments have a mixing efficiency greater than the one corresponding to the experiments with the more viscous gel shown in curve 1. Again, the reason is the greater number of turbulent plumes created when the gel viscosity is reduced (compare figs. 4 and 5) due to the decrease in the surface resistance of the gel layer. Therefore, a greater number of plumes appear and this favours the mixing process.

Looking at the evolution of the mixing efficiency (such as fig. 12) we note that the efficiency has an asymptotic behaviour and tends toward an asymptotic value in the limit that the Atwood number A tends to its maximum value. Indeed, taking the theoretical limit of the mixing efficiency in eq. (6) we arrive at the following expression:

$$\eta_{\text{limit}} = \frac{h_L - h_D}{2[2(h_L + h_G + H_0) - (h_D - h'_D)]}\,, \tag{7}$$

which is the theoretical asymptotic value. Substituting in for the parameters in our experiment, the asymptotic limit of the mixing efficiency has a value of 0.18, which is also the predicted asymptotic value.

We propose an empirical fit of exponential kind for the efficiency data. The exponential fit of the mixing efficiency is justified by the graphical behaviour shown in fig. 12. Figure 13 shows these fits made to the mixing efficiency data and they have the exponential behaviour required by fig. 12 inside our Atwood number range. The corresponding expressions are the following, for completeness we also add a series of experiments performed without a viscoelastic gel layer that, as expected, shows a higher mixing efficiency:

$$\eta_1 = 0.004 + 0.20(1 - e^{(-A/0.20)}), \qquad \eta_2 = 0.003 + 0.10(1 - e^{(-A/0.10)}), \tag{8}$$

where as usual, the subindex 1 refers to the less viscosity gel and 2 to the higher viscous one. These expressions (8) give the following empirical asymptotic values: $(\eta_1)_{\text{limit}} = 0.20$ for the less viscosity gel and $(\eta_2)_{\text{limit}} = 0.10$ for the higher viscosity gel. Therefore the predicted asymptotic value is inside the range of the empirical limits as we expected because the theoretical asymptotic limit is a general value for all CMC gel. The statistical analysis shows that this model explains about 98% of the mixing efficiency variability.

The experimental mixing process is characterized by an array of turbulent plumes which grow inside the lighter fluid layer. The plume growth is characterized by the increasing of its radius at the expense of the ambient fluid. The array of turbulent plumes generates a conical volume with no mixing inside and which is placed in the lighter layer. Therefore taking into account that there is a smaller volume for the mixing, the mixing efficiency decreases if we compare with other mixing processes which have unstable distributions of density. A brief analysis let us conclude that the volume which takes part in the mixing process can be expressed as it follows:

$$V^*_{\text{mixing}} = \left(1 - \frac{2h}{3h_L}\right), \tag{9}$$

where h is the interaction depth between plumes and h_L is the thickness of the lighter fluid layer. It is observed that the volume which takes part in the mixing decreases as the ratio between the height h and the height of the lighter layer h_L increases. Under these conditions plumes reach the greater depths without interaction. Therefore the major mixing volumes appear when plumes interact at an early stage of their evolution, because then there is still enough energy to mix at a molecular level. From the experimental data it may be inferred that the no-mixing volume oscillates between 14% and 34% and it makes an efficiency decrease which can be corrected by adding a correction factor which varies between 0.04 and 0.2.

5. – Conclusions

A new experimental model for turbulent mixing generation in a fluid system with an unstable density distribution has been presented. The main features are summarized as follows. Our experimental set-up creates an array of forced turbulent plumes whose interaction governs the phenomenon. The final result of the mixing process is the generation of a mixed layer which is stratified. This layer is separated by a stable density interface from the fraction of the lighter fluid which has not taken part in the mixing process. Because of this, the mixing process is qualified as partial. The main purpose of our subsequent analysis is to characterize this partial mixing process.

There is no other acceleration apart from gravity in this experimental method, and there are no obvious additional experimental mechanisms which would affect the energy balance in the mixing efficiency. At the physical level, the turbulent mixing process depends mainly on the initial buoyancy of the fluid system—represented by its Atwood number—and on the viscosity of the CMC gel used. In addition, the turbulent mixing occurs between miscible fluids and therefore, there is a high degree of fine scale mixing. We analyze two global properties associated with this process, the mixing efficiency η and the mixed layer height h_M.

The mixing efficiency increases with the Atwood number but decreases as the viscosity of the CMC gel is increased. The values of the mixing efficiency are less than 0.20 and tend toward an asymptotic behavior when the Atwood number tends to its maximum

value. The mixing efficiency is influenced by the fact that when the stable stratification in the mixed layer increases, more energy is consumed to work against the buoyancy forces. The mixed layer height increases as the Atwood number grows, and diminishes as the viscosity of the CMC gel grows. The global behavior of the mixed layer height *versus* the Atwood number is represented by a linear empirical fit.

We conclude that the initial distribution of plumes is very important in the global mixing efficiency and the way in which the different gel types produce more small plumes or less large ones is an important factor. For different experiments with different number and sizes of plumes and the same Atwood number the variation of the global mixing efficiency depends inversely on the volume where mixing is impossible. This volume is reduced to zero in the case of other experimental procedures such as the plate removal Rayleigh-Taylor front mixing experiments. So the reduction in mixing efficiency of about 30% observed between our results without gel and the reported higher mixing efficiency values has a simple geometrical explanation. The presence of gels produces an even stronger mixing efficiency reduction and this effect is increased as the viscosity of the gel increases.

Future research will study in a more systematic way the role of initial forcing scales and plume distribution on the mixing efficiency. This is an important effect previously described in the investigations of [6], where comparisons of numerical simulations and experiments showed the needs for correct simulations of the initial conditions because of the lack of control of plate removal. The present arrangement allows for much larger variation changing independently the size and number of holes and the viscosity of the gel to provide some initial damping.

The study of the time evolution of the convective fronts associated with the turbulent plumes, and the comparison of this time evolution with the growth of the Rayleigh-Taylor instability front is important. Other research aims to establish a possible relation between the experimental model presented here and the unstable atmospherical situations by means of the hydrodynamic and convective similarity.

* * *

The authors would like to thank J. Tijero and the Department of Chemical Engineering of the Complutense University of Madrid for invaluable help with the CMC gel and its rheological analysis. We would like to thank the research support workshops of the Complutense University of Madrid for the construction of the experimental instruments used and Prof. Velarde and the Instituto Pluridisciplinar for their help. This work was supported by Project No. PR 181/96-6757-96 granted by the Complutense University of Madrid and partly by MEC ESP2005-07551, EU-ISTC-1481 Spanish and European Proyects.

REFERENCES

[1] Itsweire Eric C., *Phys. Fluids*, **27** (1984) 764.
[2] Ratafia M., *Phys. Fluids*, **16** (1973) 1207.
[3] Read K. I., *Physica D*, **12** (1984) 45.
[4] Popil R. and Curzon F. L., *Rev. Sci. Instrum.*, **50** (1979) 1291.
[5] Böckmann M. and Müller S. C., *Phys. Rev. Lett.*, **85** (2000) 2506.
[6] Linden P. F. and Redondo J. M., *Phys. Fluids. A*, **3** (1991) 1269.
[7] Linden P. F., Redondo J. M. and Youngs D. L., *J. Fluid Mech.*, **265** (1994) 97.
[8] Sharp D. H., *Physica D*, **12** (1984) 3.

[9] Cherfils C. and Lafitte O., *Phys. Rev. E*, **62** (2000) 2967.
[10] Youngs D. L., *Physica D*, **12** (1984) 32.
[11] Youngs D. L., *Phys. Fluids A*, **3** (1991) 1312.
[12] Bizon C., Werne J., Predtechensky A. A., Julien K., McCormick W. D., Swift J. B. and Swinney H. L., *Chaos*, **7** (1997) 107.
[13] Stull R. B., *An Introduction to Boundary Layer Meteorology* (Kluwer Academic Publishers, The Netherlands) 1994.
[14] American Society for Testing and Materials, *Standard Test Methods for Sodium Carboxymethylcellulose*, Designation D1439 (1989).
[15] Brookfield Lab., *More Solutions to Sticky Problems*, AR-89 (1990).
[16] List E. J., *Ann. Rev. Fluid Mech.*, **14** (1982) 189.
[17] Redondo J. M., *Difusión Turbulenta en Fluidos Estratificados*, Ph. D. Thesis, University of Barcelona (1987).
[18] Yagüe C., *Estudio de la Mezcla Turbulenta a través de Experimentos de Laboratorio y Datos Micrometeorológicos*, Ph. D. Thesis, Complutense University of Madrid (1992).
[19] Turner J. S., *J. Fluid Mech.*, **173** (1986) 431.
[20] Fernando H., *Annu. Rev. Fluid Mech.*, **23** (1991) 455.
[21] Linden P. F., *Geophys. Astrophys. Fluid Dyn.*, **13** (1979) 3.
[22] Redondo J. M., *Mixing Efficiency of Different Kinds of Turbulent Processes and Instabilities*, edited by Linden P. F. and Redondo J. M. (CIMNE, Barcelona) 2001.
[23] Linden P. F., Redondo J. M. and Caulfield C. P., *Advances in Compressible Turbulent Mixing*, edited by Dannevik W. P., Buckingham A. C. and Leith C. E. (Princenton University) 1992.
[24] Linden P. F., *J. Fluid Mech.*, **100** (1980) 691.
[25] Linden P. F., Redondo J. M. and Youngs D. L., *J. Fluid Mech.*, **265** (1994) 97.